EXPERIMENTAL RESULTS OF DIAGNOSTICS RESPONSE FOR LONGITUDINAL PHASE SPACE

F. Frei*, V. Arsov, H. Brands, A. Saa Hernandez, R. Ischebeck, F. Löhl, B. Kalantari, R. Kalt,
B. Keil, W. Koprek, G.L. Orlandi, T. Schilcher, V. Schlott, PSI, Villigen, Switzerland

Abstract

At SwissFEL, electron bunches will be accelerated, shaped, and longitudinally compressed by different radio frequency (RF) structures (S-, C-, and X-band) in combination with magnetic chicanes. In order to meet the envisaged performance, it is planned to regulate the different RF parameters based on the signals from numerous electron beam diagnostics. Here we will present experimental results of the diagnostics response on RF phase and field amplitude variations that were obtained at the SwissFEL Injector Test Facility.

INTRODUCTION

The SwissFEL free electron laser [1] is currently under construction at the Paul Scherrer Institut. To obtain a proper and stable bunching process, certain stability requirements of different sub-systems (Laser, RF, magnets etc...) have to be reached. Diagnostics should be available to measure the related beam parameters and possibly provide this information to feedback systems, which then can be used to stabilize the beam.

In order to develop and optimize different components and procedures for SwissFEL, the 250 MeV SwissFEL Injector Test Facility (SITF) [2] is currently in operation.

To investigate the current status of the systems, a diagnostics response measurement was performed at SITF. Each RF parameter was varied separately around previously chosen initial settings. The measured responses of the diagnostics then allow conclusions on the achievable sensitivities at these initial settings. Additionally, corresponding simulations performed using the code LiTrack are presented in a separate contribution [3]. The post analysis has been done following the concept already described in detail in [4].

It is worth emphasizing that the present paper provides a snapshot of the work presently done at SITF. The systems are under continuous development and optimization to reach the ultimate goals for SwissFEL.

After a first brief overview of the systems installed at SITF, the initial settings of the RF and the diagnostic elements will be described in more detail. Based on this information, the diagnostic response measurement is described in a third section followed by a section discussing the analysis of the deduced response matrix.

SWISSFEL INJECTOR TEST FACILITY

As depicted in Fig. 1, SITF is based on an S-band radio frequency (RF) photoinjector (FINSS). A booster

LINAC consisting of normal conducting S-band RF structures (FINSB01-FINSB02-FINSB03/04) is simultaneously generating the acceleration up to 250 MeV and the necessary energy chirp for the magnetic compression in the bunch compressor (BC). To linearize the longitudinal phase space for optimal bunch compression, a fourth harmonic X-band cavity (FINXB) phased for deceleration is located in front of the bunch compressor.

Jitter and drift of field amplitude and phase of each of these accelerating cavities (subsequently referred to as actuators) affect the longitudinal phase space of the electron bunches. To measure the effect on the electron beam, SITF is equipped with longitudinal instrumentation (subsequently referred to as diagnostics) which is illustrated in Fig. 1.

For the present measurements, the bunch charge is measured with stripline beam position monitors (BPMs) that were previously calibrated against a Faraday cup and a wall-current monitor [5]. Two of these stripline BPMs (BPM-E_1, BPM-E_2) are located between the first and the second dipole of the bunch compressor, where the horizontal beam position is a measure of the mean particle energy. Furthermore, a synchrotron radiation monitor (SRM) [6] after the third dipole of the bunch compressor provides the energy distribution by imaging the incoherent synchrotron radiation onto a camera. While the position of the centroid is also a measure of the mean particle energy, the width is related to the relative energy spread.

After the bunch compressor, relative bunch length changes are measured by the bunch compression monitor (BCM). This monitor is based on coherent diffraction radiation (CDR) generated as the electron bunch passes through a hole of radius 3 mm in a 1 μm thick titanium foil. The CDR is thereafter filtered by two different "thick grid" high pass THz filters. The two different spectral bands are individually detected by two Schottky diodes. Additionally, the absolute bunch length can be measured destructively using an S-band transverse deflecting cavity (TDC). Thereby, the longitudinal profile gets vertically deflected. The bunch profile is then measured by imaging the electron distribution onto a subsequent screen.

A bunch arrival time monitor (BAM) after the bunch compressor is based on a Mach-Zehnder type modulator [7]. A high bandwidth pickup signal [8] is sampled at the zero crossing by a laser pulse. This laser pulse provides the timing reference. It is delivered in the accelerator tunnel through single-mode fiber links stabilized in length with femto second precision. The arrival time change results in deviation from the zero crossing, thus creating a modulation voltage for the electro optical modulator, which encodes the arrival time into the amplitude of the reference laser pulse.

* franziska.frei@psi.ch
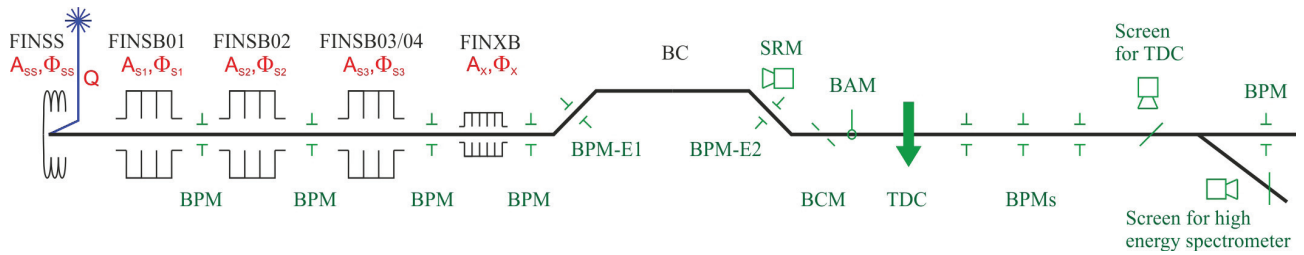
Figure 1: Scheme of the SwissFEL Injector Test Facility. The longitudinal diagnostics used through the measurement is shown in green, whereas the actuators varied are colored in red.

Ideally, one would like to have one diagnostic related to a single actuator (or vice versa). However, in reality, these beam based measurements are not independent. For example, the total CDR energy detected at the BCM is not only a measure of the relative bunch length, but is also affected by the bunch charge.

THE INITIAL SETTINGS

To investigate the diagnostic response to the different actuators, namely the RF phase, RF amplitude, and charge, the actuators are varied one by one around the initial settings (IS) listed in Table 1.

For a bunch charge of 20.5 pC, the RF parameters at the initial settings were optimized for a mean particle energy of 200 MeV and a compression factor of roughly 7 resulting in a bunch duration of 260 fs rms (see Fig. 2).
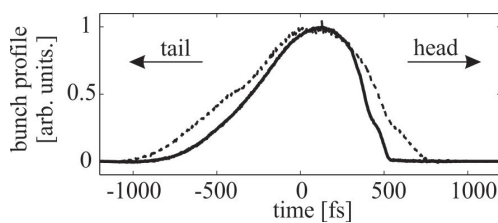
Figure 2: Solid line: Longitudinal electron bunch profile (260 fs rms) at the initial settings, measured by the TDC. Dashed line: Longitudinal electron bunch profile for a smaller compression phase.

The phase of FINSS Φ_{SS} is at the initial settings, typically set to minimize the energy spread, and the on-crest energy gain of the particle is estimated to 7 MeV. For maximal energy gain, FINSB01 is operated on-crest (phase = 0 °), with an estimated energy gain of a particle of 53.7 MeV. For the current compression scheme, the phase of FINSB02 Φ_{S2} was set slightly off-crest to -2.5 °. For this RF station, the on-crest energy gain of a particle is estimated to 70.8 MeV. However, the main energy chirp was introduced by FINSB03 at an off-crest phase of -37.5 ° with an on-crest energy gain of a particle estimated to 102.7 MeV. To linearize the compression, the fourth harmonic field FINXB with an estimated on-crest energy gain of the particle of 14.2 MeV is operated anti-on-crest with $\Phi_{XB} = 180.0$ °.

The particle energy gains for an on-crest phase are estimated based on the forward RF power at the entrance of each RF structure for the initial settings.

An RF feedback stabilizes the vector sum of the input and output RF fields measured with directional couplers. It stabilizes the RF amplitudes and phases, which might fluctuate due to temperature changes in the accelerating structures. In these measurements of the vector sum, the amplitudes are given in arbitrary units (see Table 1), while the phases are given in deg.

Table 1: Initial Settings (IS) and Variation Range of the Actuators (their stability was determined at the IS values)

Act.	IS	Var. Range	Stability
Q	20.5 pC	18.6 - 21.9 pC	0.18 pC
Φ_{SS}	148.5 °	± 1.5 °	0.039 ° (36 fs)
A_{SS}	0.4990 arb units	-2.64 - 2.04 %	0.04 %
Φ_{S1}	-0.02 °	± 1.5 °	0.022 ° (21 fs)
A_{S1}	0.3000 arb units	± 1.67 %	0.011 %
Φ_{S2}	-2.5 °	± 1.5 °	0.026 ° (24 fs)
A_{S2}	0.5950 arb units	± 0.51 %	0.0072 %
Φ_{S3}	-37.53 °	± 1.5 °	0.035 ° (32 fs)
A_{S3}	0.3309 arb units	± 6.0 %	0.056 %
Φ_{XB}	180.04 °	± 1.5 °	0.18 ° (42 fs)
A_{XB}	0.3500 arb units	± 8.6 %	0.13 %

The variation ranges of the actuators are chosen large enough to measure a clear effect on the diagnostics, but small enough to ensure linear dependencies. The resulting experimentally defined variation ranges are summarized in Table 1.

For each actuator, the stability value listed in Table 1 is the standard deviation of the measured values of 300 bunches over one minute at the initial settings. For the whole measurement, SITF was operating at the standard repetition rate of 10 Hz, but only every second bunch was measured.

For the chosen initial settings, the resolutions of the different diagnostics are listed in Table 2.

The resolution of the SRM is derived from the pixel size (40 μm) of the camera and the nominal dispersion at that position (330.9 mm). By cross calibrating the BPM-E$_1$ and BPM-E$_2$ in the bunch compressor with respect to the SRM, the dispersion at the position of these BPMs can be derived (172.6 mm). For the initial settings of 200 MeV, their spatial resolution of 8 μm results in an energy resolution roughly

Table 2: SITF Longitudinal Diagnostics and Their Resolution at the Initial Settings

Diagnostics	Quantity measured	Resolution (Δ)
BPM-E$_1$	energy diff. to the IS	9.3 keV
SRM-E	energy diff. to the IS	24 keV
SRM-Δ E/E	relative energy spread	$1.2 \cdot 10^{-4}$
BPM-E$_2$	energy diff. to the IS	9.3 keV
BCM-D1r	CDR, integr. 0.6-2 THz	1.6 mV (0.8 %)
BCM-D2r	CDR, integr. 0.26-2 THz	2.4 mV (0.6 %)
BPM-Q	mean of all BPMs	62 fC (0.3 %)
BAM-t	bunch arrival time after BC	52 fs
TDC-σ_t	bunch length	40 fs

2.6 times better than the estimated energy resolution of the SRM-E.

The resolution of the BCM is estimated according to previous correlation measurements using two identical frequency ranges for the integration. For smaller signal levels, the relative noise is slightly larger, resulting in a different relative noise for BCM-D1r and BCM-D2r.

For the BAM, the resolution is intrinsically measured from the pickup slope and the instantaneous amplitude jitter of the reference laser pulses. While the present BAM resolution at high charges (200 pC) is in the order of 10 fs, at a charge of 20.5 pC it drops to 52 fs [7].

The resolution of TDC$-\sigma_t$ is a rough estimate of comparing the measurements at the two zero-crossings in the present measurements.

Since values of actuators and diagnostics might differ by many orders of magnitude and units, the measured quantities are subsequently divided by the listed stabilities resp. resolutions.

DIAGNOSTICS RESPONSE

During the diagnostics response measurement, the actuators are varied one by one in five steps around the initial setting. For each step, all the diagnostics and actuators are read out bunch synchronously with the exception of the SRM and the TDC. While the data from the SRM was acquired simultaneously at the same five steps, the TDC measurements were done separately after all the actuators were varied since the TDC is destructive.

Throughout the measurement, the RF actuators are changed through a vector modulator via low level RF electronics and the charge was varied by rotating a polarizer in the gun-laser beam path.

As an example, the procedure is described in detail for the variation of Φ_{S3}, the phase of FINSB03 and illustrated in Fig. 3. By varying Φ_{S3}, there is not only a change in compression and bunch length expected, but also a change in energy. Furthermore, since a phase change implies a change of the curvature in phase space, this affects the energy spread as well as the bunch shape.

For the five points around the initial settings, Φ_{S3} was nominally set to [-39.03°, -30.28°, -37.53°, -36.78°, -36.03°].

The diagnostics and read back values of the actuators are recorded at 5 Hz during one minute for each set phase.

To simplify the comparison between the different measured quantities, the actuator values Φ_{S3} are divided by their rms stability of 0.035 ° and the diagnostics values are divided by the expected corresponding rms resolution, mentioned in Fig. 3 as Δ as well as in Table 2.

For each diagnostic element, Figs. 3a)-i) show the mean and standard deviation at each scan point with respect to the mean and the barely visible standard deviation of the also measured actuator Φ_{S3}.

As expected, the charge shown in g) is not affected by any change of Φ_{S3}. A very weak response might be seen for the relative energy spread by the SRM-$\Delta E/E$ in c). However the main change is observed by the diagnostics most sensitive to energy which are BPMs in the bunch compressor a) and d) and the SRM-E b). These diagnostics only show a difference from the actual energy to the original energy at the initial settings. The convention of the axis for these diagnostics is chosen to show a positive difference for an increase in energy. Since an energy change is affecting the transit time through the bunch compressor, also the BAM h) is sensitive to energy changes. While Φ_{S3} is moved towards the on-crest phase, the mean particle energy is increasing and the beam is less deflected by the dipoles in the bunch compressor. This implies a slightly shorter trajectory through the bunch compressor and therefore a negative deviation of the arrival time with respect to the measurement at the initial settings.

Furthermore, a variation in Φ_{S3} results in a change of compression that is detected by the BCMs e) and f) and the TDC i). While the phase is shifted towards the on-crest phase, the electron bunch is less compressed and the integrated energy in the two frequency ranges of the BCMs is decreased, because the coherent diffraction radiation is shifting towards lower frequencies. This is seen in Figs. 3e) and f).

The responses of individual diagnostics on the actuators are confirmed to be linear within the scan ranges. The response R_{ij} of diagnostics i with respect to the actuator j is approximated by the slope of a linear fit.

A slope of 1 corresponds to the situation where the value of the diagnostics is changing by one rms resolution, if the actuator is changed by an amount corresponding to its rms stability. This means that slopes smaller than 1 can not be measured reliably in single shot. However, slow drifts might still be detected by averaging over an appropriate number of bunches. The measured response matrix is depicted in Table 3.

DISCUSSION OF THE RESPONSE MATRIX

A very rough inspection of the response matrix in Table 3 shows, that only the charge measurement by BPM-Q is clearly sensitive to only one actuator, namely to the charge. All the other diagnostics are sensitive to more than one actuator.
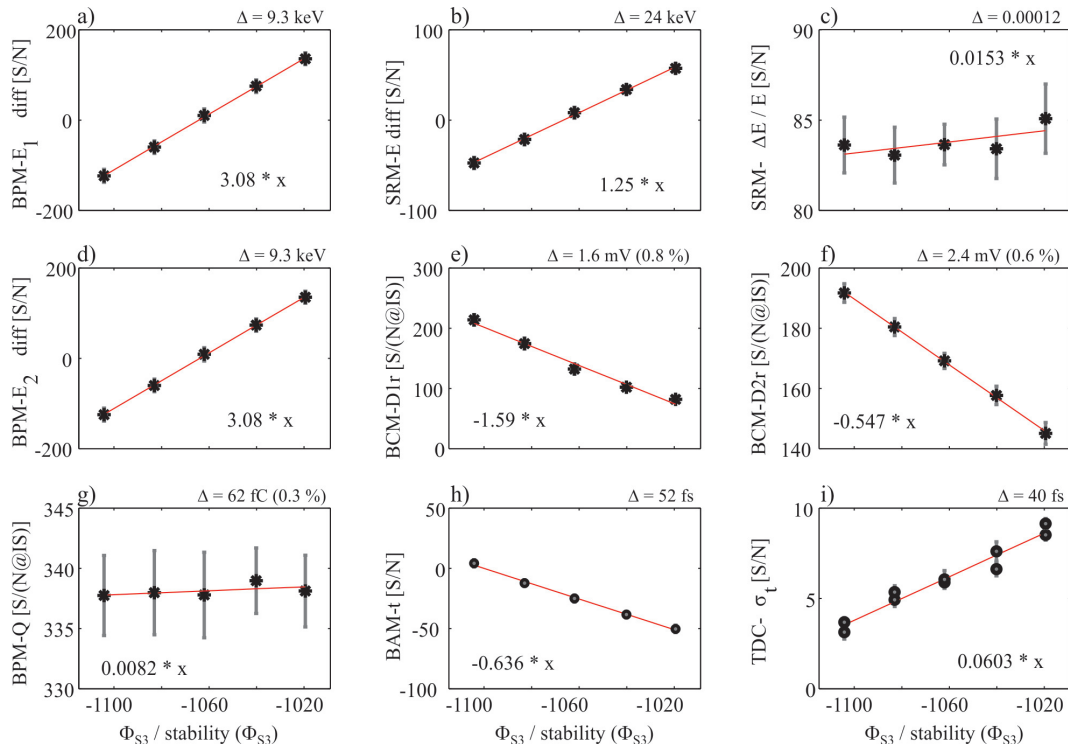
Figure 3: Phase scan of the off-crest operated accelerating structure FINSB03. Φ_{S3} is varied for 5 different settings around its IS value. The resulting measurements of the SITF longitudinal diagnostics are depicted in a) to i). The middle points correspond to the initial settings and the bars shown indicate the standard deviation. Therefore, the quantity is divided by the resolution Δ of the corresponding detector, and the RF actuator by its rms stability $0.035\,°$.

Table 3: Response matrix R of the experimentally measured values as a function of the actuators. The values measured have been divided by the measured stability of the actuators and the expected (resp. measured) resolution of the diagnostics. The bold numbers indicate the most sensitive diagnostic for each actuator according to the measurement.

	Q	Φ_{SS}	Φ_{S1}	Φ_{S2}	Φ_{S3}	Φ_{XB}	A_{SS}	A_{S1}	A_{S2}	A_{S3}	A_{XB}
BPM-E$_1$	0.11	**-1.03**	-0.07	0.07	**3.08**	0.08	**-2.93**	**0.57**	**0.38**	3.73	-1.55
SRM-E	-0.02	-0.38	-0.03	0.03	1.25	0.02	-1.13	0.23	0.16	1.50	-0.63
SRM-ΔE/E	0.08	0.05	-0.02	-0.03	0.02	0.18	-0.05	0.01	0.01	0.10	-0.03
BPM-E$_2$	0.25	**-1.03**	-0.07	0.07	**3.08**	0.05	**-2.94**	**0.57**	**0.39**	3.72	-1.56
BCM-D1r	0.98	-0.04	**-0.45**	**-0.66**	-1.59	**3.37**	0.57	-0.14	-0.08	-0.16	0.31
BCM-D2r	1.12	0.01	-0.14	-0.22	-0.55	1.01	0.20	-0.04	-0.02	-0.04	0.10
BPM-Q	**2.89**	0.09	0.01	0.00	0.01	0.04	0.08	0.00	-0.00	0.01	-0.01
BAM	-0.32	-0.02	0.01	-0.01	-0.63	0.01	-0.13	-0.12	-0.07	-0.72	0.31
TDC - σ$_t$	-	0.00	0.02	0.02	0.06	-0.17	-0.01	0.00	0.01	0.00	-0.01

Since the responses of each diagnostic on each actuator is linear, simultaneous variations of all parameters can be represented as a linear combination of the individual variations. Therefore, the response matrix can be analyzed using the method of singular value decomposition (SVD) [9].

For this purpose, the response matrix R can be decomposed into three matrices according to

$$R = U \cdot \Sigma \cdot V^T, \qquad (1)$$

where the matrix Σ is a diagonal matrix, containing the singular values of R. By convention, they are sorted by descending order, as depicted in Table 4. Each singular value corresponds to the weighting factor of the related mode. The corresponding mode is derived from the left singular vectors of R contained in U (describing the diagnostics in Table 5) and the right singular vectors of R contained in V (describing the actuators in Table 6). Since the singular values for mode 7-9 are very small compared to the first 6 modes, in

Table 5 and 6 only the first 7 singular vectors are shown for better understanding.

Table 4: Matrix Σ, containing the singular values of R. They describe the importance of the corresponding singular vectors in U, resp. V.

	1	2	3	4	5	6	7	8	9
1	**8.96**	0	0	0	0	0	0	0	0
2	0	**4.22**	0	0	0	0	0	0	0
3	0	0	**2.70**	0	0	0	0	0	0
4	0	0	0	**0.62**	0	0	0	0	0
5	0	0	0	0	**0.08**	0	0	0	0
6	0	0	0	0	0	**0.06**	0	0	0
7	0	0	0	0	0	0	0.01	0	0
8	0	0	0	0	0	0	0	0.01	0
9	0	0	0	0	0	0	0	0	0.01

Table 5: Matrix U, containing the first seven left singular vectors of R as columns. They describe the diagnostics and are sorted according to their importance.

	1	2	3	4	5	6	7
BPM-E$_1$	**-0.67**	0.11	-0.07	-0.06	-0.03	-0.10	0.37
SRM-E	**-0.27**	0.03	-0.04	0.06	0.17	0.06	0.42
SRM-ΔE/E	-0.01	0.05	-0.02	0.03	**0.89**	**0.39**	-0.10
BPM-E$_2$	**-0.67**	0.12	-0.02	-0.10	-0.05	0.07	-0.54
BCM-D1r	0.17	**0.82**	**-0.46**	0.03	0.06	-0.26	-0.09
BCM-D2r	0.06	**0.36**	0.11	-0.05	**-0.36**	**0.81**	0.22
BPM-Q	0.00	**0.40**	**0.87**	-0.10	0.11	-0.24	-0.01
BAM	0.09	-0.05	-0.11	**-0.98**	0.06	-0.01	0.04
TDC - σ$_t$	-0.01	-0.03	0.04	0.00	-0.14	0.20	-0.57

Mode number 1 is primarily acting on the mean particle energy. The first row in U implies that this mode is basically measured by the BPM-E. The corresponding actuators are mainly A_{S3}, Φ_{S3} and A_{SS}. A slightly lower impact on the energy is given by A_{XB}. Since FINXB is operated anti-on-crest, this coefficient has the opposite sign compared to the coefficient for the amplitude of FINSB03.

Mode number 2 is describing a combined compression-charge mode, mainly detected by the BCM-D1r and the BPM-Q (column 2 in U). The leading actuators (column 2 in V) are the phase of FINXB and the charge. A smaller influence is given by the phases of FINSB03 and FINSB02 as well as the amplitude of FINSB03.

Since BCM-D1r is integrating the CDR energy in a narrower spectral range starting at a higher frequency than BCM-D2r (see Table 2) , the relative change of the detected CDR is higher than for BCM-D2r, thus resulting in a higher sensitivity with respect to compression.

Table 6: Matrix V, containing the first seven right singular vectors of R as columns. They describe the actuators and are sorted according to their importance.

	1	2	3	4	5	6	7
Q	-0.00	**0.57**	**0.82**	-0.06	-0.02	-0.01	-0.00
Φ_{SS}	0.16	-0.05	0.08	0.23	**0.86**	**0.41**	0.04
Φ_{S1}	0.00	-0.10	0.08	-0.01	0.08	-0.08	-0.07
Φ_{S2}	-0.03	-0.14	0.10	-0.02	0.13	**-0.35**	0.84
Φ_{S3}	**-0.53**	-0.18	0.14	**0.33**	0.28	**-0.60**	-0.27
Φ_{XB}	0.06	**0.75**	**-0.52**	0.07	0.21	-0.30	0.02
A_{SS}	**0.48**	-0.03	0.07	**0.82**	-0.27	-0.10	0.02
A_{S1}	-0.10	0.00	0.00	0.06	-0.07	0.10	-0.01
A_{S2}	-0.06	0.00	-0.00	0.04	-0.00	0.09	0.02
A_{S3}	**-0.61**	0.19	-0.11	**0.35**	-0.19	**0.46**	0.35
A_{XB}	0.26	-0.02	0.00	-0.16	0.02	-0.13	0.29

Mode number 3 is also describing a combined charge-compression mode with the same contributors as mode number 2, but now primarily acting on the charge. In contrast to mode 2, the relative signs of charge and compressions are opposite.

Mode number 4 with a singular value already more then 10 times smaller then the first one, is describing the arrival time. This is exclusively detected by the BAM. The corresponding main actuator is given by the amplitude of FINSS and, much weaker, by the phase and amplitude of FINSB03.

Mode number 5 having a singular value which is roughly 100 times smaller then the first mode, is only contributing very little to the overall response. However, column 5 in U is indicating that mainly the relative energy spread is affected with a slight contribution of also BCM-D2r by the corresponding main actuator of the phase of FINSS (column 5 in V).

The remaining singular values are so small, that they are probably dominated by noise and have no constructive impact on the response matrix. Therefore, columns 8 and 9 of the matrices U and V are not shown for better understanding.

CONCLUSION AND OUTLOOK

A diagnostics response matrix was successfully measured at one working point of the SITF. As expected, the beam based measurements of the different diagnostics are not decoupled. This implies that different beam parameters can only be stabilized by using an appropriate procedure based on different diagnostics.

This can be seen for example in mode number 1, dedicated to energy. There is not only one actuator mainly affecting the energy, but the gun amplitude A_{SS} as well as the amplitude of the accelerating S-band cavity A_{S3} and the compression

phase Φ_{S3} are contributing in the same order of magnitude relative to their stability.

It is worth underlining that the specific responses R_{ij} are determined based on the measured stabilities of the actuators. These stabilities vary from RF station to RF station as listed in Table 1. If these stabilities change, for example because the temperature stabilisation of an RF cavity is improved, this would affect all entries in the response matrix. In particular the relative importance of the different actuators might then change in the present representation.

The charge and compression modes (modes number 2 and 3) might be disentangled by compensating the influence of varying charge on the bunch compression monitor in the data processing. This would lead to zeros in the response matrix for $R_{BCM-D1r,Q}$ and $R_{BCM-D2r,Q}$. In consequence, mode number 2 would be dedicated to compression, with the leading actuator of the X-band phase followed by the S-band compression phase and the S-band amplitude. Mode number 3 would be purely sensitive to charge.

As can be seen from the response matrix R, the two BPMs in the bunch compressor as well as the centroid of the synchrotron radiation monitor SRM-E are redundant measurements with a higher accuracy for the BPMs. However, the BPMs only allow to measure the center of mass of the particle energy distribution in the electron bunch. In contrast, the synchrotron radiation monitor provides additional information on the longitudinal phase space projected onto the energy axis. The width of this distribution (the relative energy spread) is the main measure used in mode number 5.

According to the response matrix, the BCMs, sensitive to bunch length changes, do not allow for a clear distinction between a change in the compression phase Φ_{S3} and Φ_{XB}. To solve this ambiguity, the choice of spectral filters could probably be improved further, or a more direct measure of the curvature in phase space could be beneficial.This could possibly be implemented using not only the centroid and the width at the synchrotron radiation monitor, but also some information about the measured shape and their asymmetry.

As a further option, instead of measuring the asymmetry of the longitudinal phase space projected onto the energy axis, the equivalent information is expected for a direct measure of the asymmetry in the temporal profile of the electron bunch.

It is worth noting that there are further effects affecting a proper and stable bunching process not accounted for in these measurements presented here. Among others these are laser arrival time on the cathode, fluctuations in the longitudinal laser pulse profile or the stability of the magnetic fields.

The presented diagnostic response measurement serves first and foremost as a response study of the current diagnostics installed at SITF. In particular, there were more actuators than linear independent diagnostics available. If this approach of SVD would be used for regulation, the different weighting factors would probably need to be optimized experimentally. Furthermore, for slow regulations, it could be important to account for drifts of the diagnostics which were neglected throughout this paper.

REFERENCES

[1] R. Ganter (ed.), "SwissFEL Conceptual Design Report", PSI Bericht, 10-04, 2010, `ftp://ftp.psi.ch/psi/SwissFEL_CDR/SwissFEL_CDR_V20_23.04.12.pdf`

[2] M. Pedrozzi (ed.), "SwissFEL Injector Conceptual Design Report", PSI Bericht, 10-05, 2010, `http://www.psi.ch/swissfel/CurrentSwissFELPublicationsEN/SwissFEL_Injector_CDR_310810.pdf`

[3] A. Saa Hernandez et al., "Longitudinal Response Matrix Simulations for the SwissFEL Injector Test Facility", in *These Proceedings: Proc. 36th Int. Free-Electron Laser Conf.*, Basel, 2014, THP097.

[4] R. Ischebeck et al., "Response Matrix of Longitudinal Instrumentation in SwissFEL", in *Proc. 33rd Int. Free-Electron Laser Conf.*, Schanghai, 2011, FROA4.

[5] B. Keil et al., "Comissioning of the Resonant Stripline BPM System of the SwissFEL Test Injector", in *Proc. 33rd Int. Free-Electron Laser Conf.*, Shanghai, 2011, pp. 652-655.

[6] G.L. Orlandi et al., "Bunch-Compressor Transverse Profile Monitors of the SwissFEL Injector Test Facility", in *Proc. Int. Beam Instrumentation Conf.*, Tsukuba, 2012, pp. 271-275.

[7] V. Arsov et al., "Commissioning and Results from the Bunch Arrival-time Monitor Downstream the Bunch Compressor at the SwissFEL Test Injector", in *These Proceedings: Proc. 36th Int. Free-Electron Laser Conf.*, Basel, 2014, THP085.

[8] A. Angelovski et al., "High bandwidth pickup design for bunch arrival-time monitors for free-electron laser", in Phys. Rev. ST Accel. Beams 15, 112803, 2012.

[9] I. Bronstein et al., *Taschenbuch der Mathematik*, (Verlag Harri Deutsch, 2008), 7th edition.